Locally Measured Neuronal Correlates of Functional MRI Signals

4

Amir Shmuel and Alexander Maier

4.1 Blood Oxygenation Level-Dependent (BOLD) Signals

The majority of functional brain imaging studies in humans rely on functional magnetic resonance imaging (fMRI) (Bandettini et al. 1992; Kwong et al. 1992; Ogawa et al. 1992). The most commonly used fMRI contrast is the BOLD signal (Ogawa et al. 1990). The BOLD signal is inversely proportional to the local content of deoxyhemoglobin (deoxyHb). When neuronal activity increases, local arterial cerebral blood flow (CBF) increases to a larger extent than the metabolic increase in oxygen consumption (Fox and Raichle 1986; Hoge et al. 1999). In other words, following increased neuronal activity, CBF overcompensates for the increased need for oxygenated blood. As a result, deoxyHb content drops within local capillaries, venules, and draining veins. This process can be monitored via MRI by tracking the changing magnitude of the BOLD signal over time (Buxton et al. 2004). fMRI signals are only indirect measures of neuronal activity, which rely on intermediary processes such as neurovascular coupling and MR contrast. Therefore, the interpretation of fMRI data relies heavily on inferences about how this hemodynamic response relates to local changes in neural activity. In order to fully utilize fMRI as an effective method to study brain function, it is vital to understand how metabolic and hemodynamic responses relate to the underlying neural activity.

A. Shmuel (✉)
McConnell Brain Imaging Centre, Montreal Neurological Institute, McGill University, Montreal, QC, Canada
e-mail: amir.shmuel@mcgill.ca

A. Maier
Department of Psychology, Vanderbilt University, Nashville, TN, USA
e-mail: alex.maier@vanderbilt.edu

C. Mulert, L. Lemieux (eds.), *EEG - fMRI*,
https://doi.org/10.1007/978-3-031-07121-8_4

4.2 Extracellular Neurophysiological Signals

Neurons receive inputs via synapses that are located at their soma and their dendrites. These inputs take the form of two post-synaptic potentials, excitatory and inhibitory post-synaptic potentials (EPSPs and IPSPs), respectively. These post-synaptic potentials can be measured directly using intracellular or patch-clamp techniques. However, there are significant technical challenges associated with these measurements such as the requirement for complete immobilization of the sampled tissue. Thus, most in vivo studies resort to measuring electric activity in the extracellular space. Post-synaptic *input* potentials propagate along the neuron's dendrites toward its soma. Depending on the ratio of concurrent excitatory to inhibitory synaptic inputs, as well as on the synchronization between excitatory inputs, action potentials (spikes) may get initiated at the soma's axon hillock. Action potentials propagate along the axon toward the cell's pre-synaptic axonal terminals, where they release the all-or-none *output* of the neuron to its recipients. This signaling is done through chemical neurotransmitters or neuromodulators that diffuse from vesicles into the synaptic cleft.

The vast majority of intracortical neurophysiological measurements (recordings) are based on extracellular voltages. Extracellular recordings measure electric signals within the extracellular medium, which reflect both synaptic and spiking activities. However, extracellular recordings cannot resolve the membrane potentials of isolated neurons. When inactive, the majority of neurons harbor a voltage gradient of about 60–70 mV across their lipid membranes. Neurons maintain this voltage gradient by actively moving certain anions from the extracellular medium into their cell bodies via specialized ion pump membrane proteins. The resulting potential difference between a neuron's intracellular space and the extracellular medium is called the "resting potential." Put differently, the inside of an inactive neuron contains more negative charge than the extracellular medium. When there is a membrane potential difference between two distinct regions of the neuron, current will start to flow between them. This current flow within neurons causes a canceling return current in the extracellular space to flow in the opposite direction. Importantly, each of these currents remains isolated within its respective compartment.

In contrast, neuronal activity (both the synaptic input and the axonal output in the form of action potentials) takes the form of ionic current flow *between* the extracellular fluid and intracellular compartments. The net negative (anionic) influx into an inactive neuron hyperpolarizes that cell. The result of such currents is that the neuron's inside is even more negative than before, which makes its activation less likely. Hyperpolarizing inputs thus act as inhibitory currents. Physiologically, these kinds of anionic currents take the form of inhibitory post-synaptic potentials (IPSPs).

Cationic influx into neurons, on the other hand, depolarizes neurons until they reach a threshold of activation. Once this threshold is reached, the neuron will initiate an action potential. Physiologically, excitatory currents occur at synaptic sites in the form of excitatory post-synaptic potentials or (EPSPs).

By convention, a site through which currents either enter or leave a given system is termed a current source or a current sink, respectively. Note that the sign (i.e.,

direction) of the current is dependent on the perspective of the observer. Consequently, the definition of what constitutes a current sink or source is also relative. When neuronal activity is concerned, however, it has become customary to refer to excitatory (depolarizing) currents as a current sink. Thus, neuronal current sinks are typically indicative of a site of synaptic excitation. To close the current loop, other regions of the same neuron will undergo net effluxes of positive ions. This current source thus leads to passive return currents (Nicholson 1973). The electrical dipole that results from the spatial separation between the current sink and source forms the basis of the time-varying voltage difference that can be measured with nearby microelectrodes. In other words, the microscopic ionic fluxes across the nerve cell membrane that arise from neuronal activation sum to extracellular voltage fluctuations that can be recorded as the extracellular broad-band signal.

Local field potentials (LFPs) refer to the bulk of extracellular voltage changes established by activity in a large number of neurons nearby a microelectrode placed within the extracellular space in vivo (Fig. 4.1). The highest magnitude of the

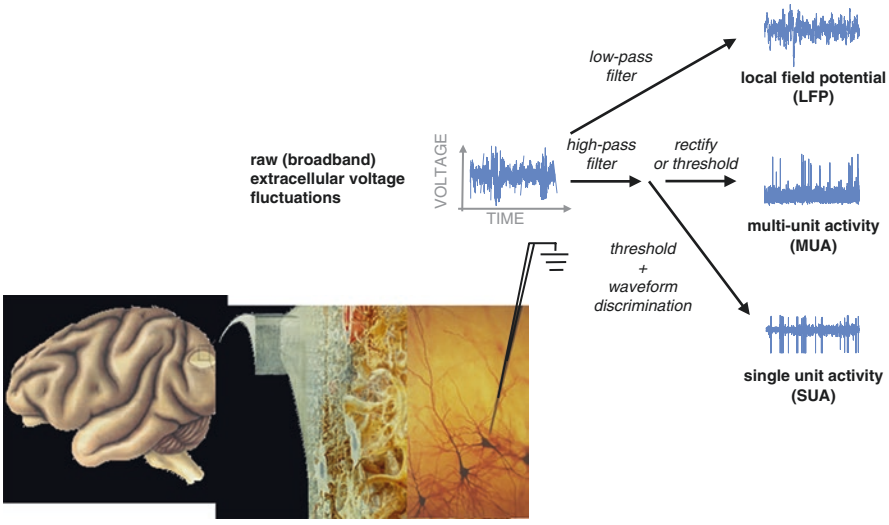

Fig. 4.1 Types of extracellular neurophysiological signals. Neurophysiologists commonly discriminate three major classes of signals that can be measured with microelectrodes placed inside the neuropil. (1) Depending on the material, geometry, and exact position of the probe, it is possible to isolate action potentials (spikes) of one or more isolated neurons. This single-unit activity (SUA) is quantified in a three-stage process. First, using band-limiting filters, the raw extracellular voltage gets narrowed down to a frequency band that matches the bandwidth of action potentials (~1 kHz). Next, the occurrence of individual impulses gets marked by determining the time points at which the signal exceeded a certain threshold. In the final step, waveform analysis gets applied to discriminate individual neurons. (2) The activity of larger populations of neurons (multi-unit activity, MUA) can be assessed by band-limiting the raw data to the frequency range of spiking activity, followed by either indiscriminate thresholding or by simple full-wave rectification in order to obtain the time-varying envelope of the band-limited signal. (3) Band-limiting the raw data into frequencies below the spectral range of spiking activity results in a signal called the local field potential or LFP

time-varying variance of extracellular voltage fluctuations occurs in the lowest frequency range. LFP magnitude decreases exponentially for increased LFP frequency. Given this predominance of low-frequency power in their spectral composition, LFPs are usually analyzed in reference to the frequency domain (i.e., in time-frequency analysis or in frequency bands also used in classical EEG: delta, theta, alpha, beta, and gamma; Fig. 4.2). Importantly, LFPs consist of a continuous spectrum rather than a few discrete frequencies. Under some conditions, LFPs exhibit repeating patterns for limited periods of time, thus resembling actual oscillations at set frequencies. However, such oscillatory LFPs are the exception rather than the norm. Most frequently, cortical LFPs exhibit no sustained periodicity and therefore are better characterized as irregular fluctuations.

LFPs have proven to be a useful measure of local neural activity as they can provide an indication of (mostly) synaptic processes without the need for

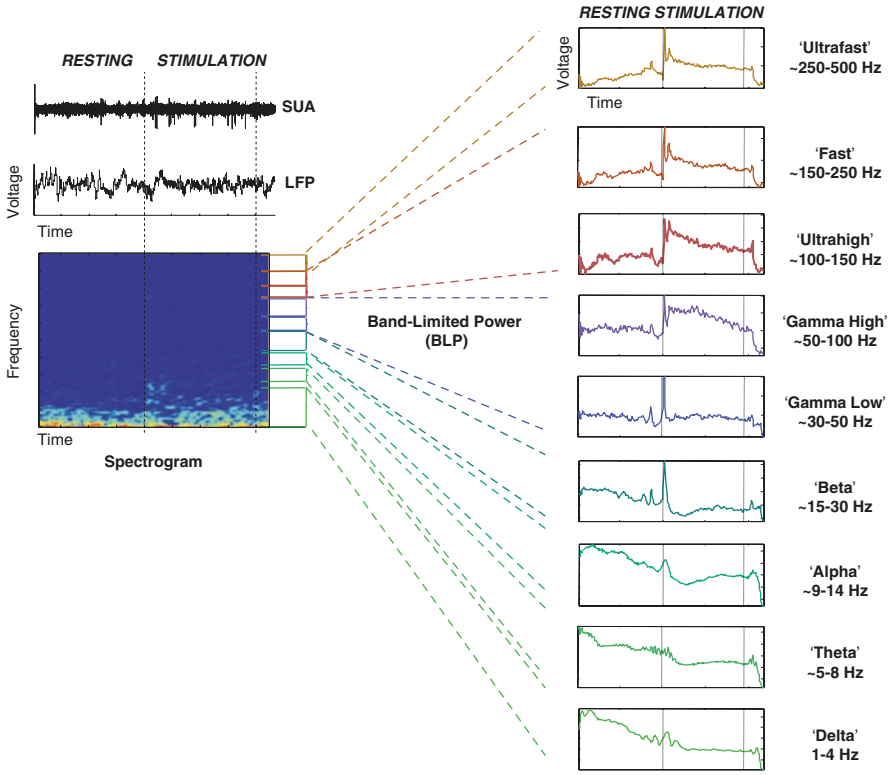

Fig. 4.2 Decomposition of LFP into frequency bands. The LFP represents a complex signal that is dominated by slow-varying, large-amplitude fluctuations. Averaging raw LFP, although informative, thus tends to over-represent its low-frequency content. A common way to circumvent this bias is to break up the signal into its frequency components and study their evolution over time. This can be done either (1) by band-bass filtering the LFP into discrete frequency bands and estimating the band-limited power (BLP) or by (2) directly transforming the signal into the frequency domain using the Fourier transform or related mathematical techniques. *SUA*, single-unit activity

intracellular recordings. Nonetheless, LFPs are not perfect indicators of neuronal activity since LFPs arise from a multitude of neural events that cannot be easily disentangled. Specifically, LFPs' amplitudes depend on multiple factors, such as the magnitude and spatial distribution of the underlying current sources and sinks, as well as on their temporal synchrony. The functional anatomy, relative position, and orientation of activated cells further influence the measured LFPs. For instance, stimulation of Purkinje cells in the cerebellum gives rise to large, coherent LFPs. The same can be found for pyramidal cells in the cerebral cortex because their dendrites are predominantly oriented parallel to each other, which supports linear spatial summation of voltages. Some interneurons, on the other hand, do not contribute to LFPs in the same way, as their dendrites are distributed in a radial, star-shaped pattern (Lauritzen 2005). Moreover, according to the relative timing of the neurons' activation and their relative geometrical arrangement, field potentials generated by two or more neurons may add up or cancel each other across the extracellular space (for reviews on field potentials, see Freeman (1975) and Logothetis (2002)).

With most microelectrodes of suitable geometry placed in the close vicinity of neurons, the slow-varying LFPs will be recorded simultaneously with the action potentials of nearby neurons. Analytically, LFPs can be dissociated from spiking activity by temporal filtering of the raw broad-band signal into two bands of frequencies above ~300 Hz and below ~150 Hz to separate the spiking activity of neurons (multi-unit activity, MUA) and LFPs, respectively (Figs. 4.1 and 4.2).

Separating LFPs and spiking-related activity by their frequency content, as described above, can be justified theoretically (Logothetis 2002). Both EPSPs and IPSPs are relatively slow events (10–100 ms long). In contrast, action potentials happen rather fast (0.4–2 ms long). As a direct consequence, the power spectra for synaptic events are predominated by much lower frequencies than that of spikes. Specifically, the average frequency spectrum of action potentials exhibits a peak around 1 kHz, while the frequency spectra of simulated EPSPs peak below 150 Hz. The same split across frequencies is found when comparing the frequency spectrum of a series of scattered synaptic events to the spectrum of spiking events.

Combined intra- and extracellular measurements further support the notion that LFPs have a synaptic-dendritic origin (e.g., Pedemonte et al. 1998). Moreover, current source density (CSD) analysis, a neurophysiological measurement technique that allows for the quantification of current flow within the neuropil, indicates that LFPs correspond to a weighted average of synchronized dendro-somatic activity from neurons within 0.5–3 mm of the electrode tip (Mitzdorf 1987; Juergens et al. 1999).

To summarize, there is converging theoretical and empirical evidence to support the concept that LFPs mainly reflect synaptic events, including synchronized synaptic input from afferent fibers as well as synaptic activity originating from local neurons. Specifically, LFPs seem to represent the summed synaptic activity of neurons that are located within ~2 mm of the recording electrode tip. In contrast, MUA seems to correspond to a weighted sum of action potentials within a ~200 μm radius from the electrode tip. The MUA is deemed to be dominated by the action potentials of pyramidal cells. However, action potentials from axons of passage, dendrites, and local interneurons likely also play a role.

It is important to note that neocortical neurons are not spread out randomly. Instead, cortical neurons are grouped within a well-ordered layered layout that largely repeats itself across the cortical mantle. This cortical lamination can be made visible using a variety of histological staining techniques. The exact number of layers that can be discerned depends on the type of histological stain and varies between cortical areas and individual species (DeFelipe et al. 2002). This variability in cortical layer count has prompted neuroanatomists to propose a variety of slightly different labeling schemes (Billings-Gagliardi et al. 1974; Marín-Padilla 1998). However, the current consensus follows neuroanatomist Korbinian Brodmann's (1868–1918) original plan of dividing the neocortex into six major laminae. These six basic cortical layers are often grouped further into three major laminar domains. In particular, layer 4 and its various sublayers are commonly referred to as the "granular layers" due to the predominance of small neurons that give rise to a fine-grained appearance in some histological stains. Accordingly, superficial layers 1–3 have been termed the "supragranular" layers, while deeper layers 5 and 6 are referred to as "infragranular" layers. Some neocortical areas seem to harbor no or little layer 4 and are thus referred to as "agranular cortex." Cortical areas with less than four layers (such as the olfactory cortex and the hippocampus) are thought to be distinct from the neocortex and distinguished as "allocortex," accordingly.

The reasoning for the above labeling scheme is that the connection patterns between these three main laminar compartments, as well as their interconnections with other cortical and subcortical sites, share a common scheme across the mammalian neocortex (but see Haug 1987; Horton and Adams 2005; Nelson 2002). This observation has given rise to the hypothesis that there is a "canonical" blueprint to the cortical laminar circuitry that is constant across the cortical sheet (Hubel and Wiesel 1974; Rockel et al. 1980). The signal flow across this stereotypical microcircuit has been mapped using a combination of anatomical and physiological techniques (e.g., Bode-Greuel et al. 1987; Nowak et al. 1995). A consensus model derived from these studies (Douglas et al. 1989; Douglas and Martin 2004; Bannister 2005; Lübke and Feldmeyer 2007; Felleman and Van Essen 1991; Sotero et al. 2010) suggests that the bulk of the ascending signals arrives in the granular compartment. Granular neurons then pass these signals onto neurons in the supragranular layers, where the ascending signals are integrated with other cortico-cortical and subcortical inputs. The supragranular neurons then project these integrated signals to other cortical areas as well as to neurons in the infragranular layers. Infragranular neurons back-project to the granular and supragranular layers, thus forming a reverberating loop between the superficial and deep cortical layers. Infragranular neurons additionally project to thalamic nuclei and other subcortical structures (Thomson and Bannister 2003).

While this stereotypical template of excitatory cortical laminar circuitry is still an idealized concept (Silberberg et al. 2002; Herculano-Houzel et al. 2008; Rakic 2008), it has been a popular concept for macroscopic models of cortical connectivity. Following the logic outlined above, any inter-cortical projections that originate outside granular layer 4 and terminate in layer 4 of another area are defined as ascending or "feedforward." Projections that innervate another area by sparing

granular layer 4 are characterized as descending or "feedback" (Rockland and Drash 1996). Using this framework, one can derive a rough wiring diagram of the functional "circuitry" between cortical areas based on their laminar interconnections. The popular "distributed but hierarchical" schematic that is commonly applied to cortical sensory areas such as the visual system is mainly based on this organizational principle (Felleman and Van Essen 1991).

The anatomical distinction of cortical layers outlined above is of great importance for the interpretation of fMRI signals. For one, fMRI has followed a steady trend toward resolving activity within and between cortical layers (e.g., Self et al. 2019; Lawrence et al. 2017; Trampel et al. 2019; Stephan et al. 2019; Huber et al. 2017), as its spatial resolution continues to improve (e.g., Mittmann et al. 2011; Polimeni et al. 2010; Goense et al. 2016; Chaimow et al. 2018). However, the laminar differences of cortical organization outlined above are also relevant for fMRI data that—in the majority of studies—lack the spatial precision to differentiate between these laminae. In line with the anatomical separation of neurons across cortical layers, functional activation differs along the same microscopic scales (Schroeder et al. 1998; Snodderly and Gur 1995; Bollimunta et al. 2008; Hansen and Dragoi 2011; Ninomiya et al. 2015; Sotero et al. 2015; Engel et al. 2016; Klein et al. 2016; Dougherty et al. 2017; van Kerkoerle et al. 2017; Hembrook-Short et al. 2017; Nandy et al. 2017; Cox et al. 2019; Sajad et al. 2019). For example, recent work has shown that the LFPs within the upper cortical layers (1–4) of the monkey visual cortex share little commonality with LFPs in the lower two cortical layers. This functional separation holds for both ongoing activity and sensory stimulation (Maier et al. 2010, 2011; Buffalo et al. 2011; Bastos et al. 2018). Likewise, the LFPs within cortical layers 1–5 of the rat somatosensory show different synchronization patterns relative to the LFPs in layer 6 (Sotero et al. 2015). These results suggest that the heterogeneity of neuronal activity along the cortical thickness needs to be taken into account when comparing neuronal signals to fMRI measurements (Maier et al. 2014).

4.3 Relationship Between Neuronal Activity and fMRI Signals

In the temporal domain, the BOLD response appears as a sluggish, low-pass filtered version of the neurophysiological response. A straightforward explanation for this observation is that changes in blood flow occur on a much slower time scale than changes in neuronal activity: BOLD responses to brief, discrete stimulation transpire within hundreds of milliseconds to seconds, while neurophysiological responses typically take place within milliseconds or tens of milliseconds. The neuronal response to a visual stimulus in the primary visual cortex (V1), for example, occurs within 20–50 ms and peaks within 30–70 ms following the onset of stimulation (Maunsell and Gibson 1992). The onset of the associated vascular response lags 1.5–2.5 s behind this neuronal response. The measured onset of the corresponding BOLD response depends on the specific experimental paradigm, the signal-to-noise

ratio (SNR), the response magnitude, and analysis parameters. Characteristically, peak blood flow and maximal BOLD response are measured 5–6 s following exposure to a short stimulus. Hence, a vascular response to a synaptic input may still be developing by the time a second or more stimuli excite the active cortical region. Whenever such a temporal overlap between responses occurs, the vascular response to a stimulus may be influenced by preceding stimuli (Lauritzen 2005).

When it comes to space, the resolution of fMRI signals is influenced by both the choice of fMRI contrast and the strength of the magnetic field. It also depends on which aspect of the brain's vasculature is probed (e.g., capillaries, venules, or veins). The point-spread function (i.e., "blur") of the T2* BOLD response in human visual area V1 has been estimated as ~3.5 mm at 1.5 T (Engel et al. 1997) and less than 2 mm at 7 T (Shmuel et al. 2007). The point-spread function of T2 and T2* BOLD responses at 7 T relative to metabolic activity has been estimated as ~0.8 and ~1.0 mm, respectively (c.

4.4 Correlations Between Neurophysiological Signals and fMRI Responses

The vast majority of studies analyzing the link between neuronal, metabolic, and hemodynamic responses found a monotonic (or even linear) increase in metabolic and hemodynamic activity following increases in neural activity. For example, relative changes in the level of blood oxygenation in the cat primary visual cortex (area 18) are proportional to increases in neuronal activity during the first phase (the so-called initial dip) of the associated metabolic and hemodynamic response (Shmuel and Grinvald 1996; Fig. 4.3a). In the same vein, in rat somatosensory cortex, the rate of oxygen consumption is proportional to increases in neuronal activity during the late phase of the hemodynamic response (Smith et al. 2002; Fig. 4.3b). It has also been shown that the CBF response to stimulation of climbing fibers in the rat cerebellum is proportional to the integrated neuronal responses induced by that stimulation (Mathiesen et al. 1998).

The amplitudes of sensory (forepaw)-evoked potentials were found to linearly correlate with the BOLD responses in rat somatosensory cortex across several stimulus frequencies (Brinker et al. 1999). An analogous conclusion was reached for humans after observing the hemodynamic response to stimulation of the median nerve using different stimulus intensities (Arthurs and Boniface 2003). Likewise, in monkeys, visual stimuli with varying luminance contrasts elicited BOLD responses that were proportional to the corresponding increases in neuronal activity (Logothetis et al. 2001).

In addition to the linear relationship between neurophysiological and BOLD responses observed in the studies outlined above, other studies found evidence for nonlinear relationships between these two measures. The CBF response to stimulation of parallel fibers within the cerebellum has shown a sigmoidal relation to the summated increases in neuronal activity (Mathiesen et al. 1998; Fig. 4.4).

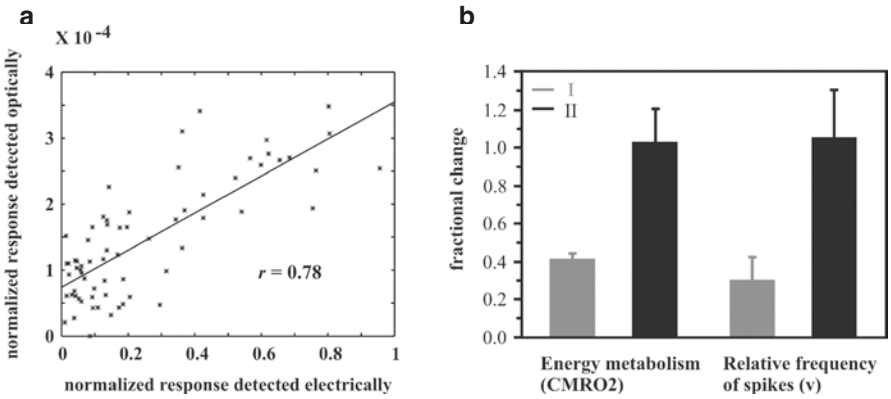

Fig. 4.3 Association between oxygen consumption and spiking activity. (**a**) Correlation between changes in blood oxygenation measured optically and the underlying action potential activity. These data were taken during the initial phase ("initial dip") of the response. Linear regression was used to generate the best linear fit to the data, which shows a high degree of linearity. (Modified from Fig. 7 of Shmuel and Grinvald (1996) with permission). (**b**) Stimulation of the rat forepaw led to comparative changes in oxygen consumption and spiking activity. Responses obtained from baseline conditions I and II are shown in *grey* and *black*, respectively. The baseline condition II was lowered by ~30% from baseline condition I due to a higher dosage of α-chloralose; however, the incremental response from condition II was larger. In both modalities, oxygen metabolism and spiking activity, the same levels of activation were approximately reached upon stimulation from the two different starting baseline levels. CMRO2, cerebral metabolic rate of oxygen. (Modified from Fig. 3 of Smith et al. (2002) with permission)

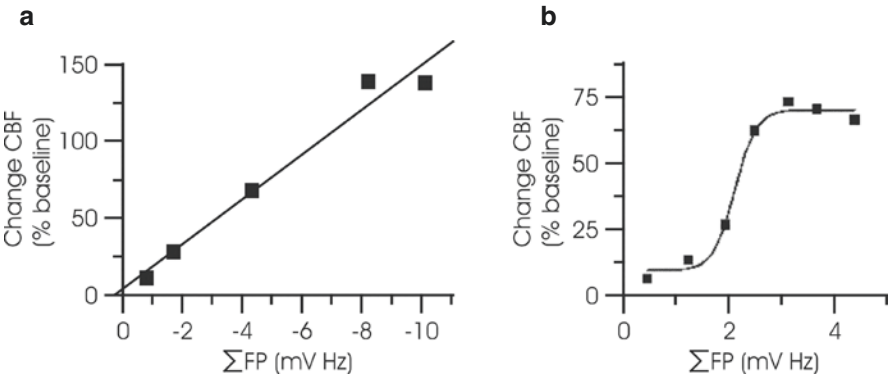

Fig. 4.4 Relationship between neuronal and hemodynamic responses in the rat cerebellum. (**a**) Frequency-dependent CBF increases in response to climbing fiber stimulation are correlated with the sum of active and passive post-synaptic activity. The figure presents the scatter plot of increases in CBF vs. summed field potentials (i.e., the product of field potential amplitudes and stimulation frequency). The line demonstrates the results of linear regression ($r = -0.985$, $P = 0.0022$). (**b**) Stimulation of parallel fibers at increasing frequencies leads to increases in summed field potentials and increases in CBF responses. The figure presents increases in CBF (ordinate) vs. summed field potentials (abscissa) from one rat, illustrating a sigmoidal relationship between the two variables. Both panels were modified from Mathiesen et al. (1998) (Figs. 4d and 5d) with permission

Devor et al. (2003) demonstrated a nonlinear relationship between neuronal and hemodynamic responses by combining optical measurements of hemodynamic signals with simultaneous recordings of neural activity. Specifically, in an event-related paradigm, the hemodynamic response continued to increase with stimulus intensity beyond the point of saturation of the electrical activity. Jones et al. (2004) and Sheth et al. (2004) reported similar observations. In the latter study, nonlinear models provided a better fit than linear models for the observed neurovascular coupling in the rat somatosensory cortex. Hoffmeyer et al. (2007) examined neurovascular coupling in rat sensory cortices in response to direct stimulation of transcallosal pathways. They showed that there is an exponential relationship between CBF responses and the summed amplitudes of neuronal activity. Nielsen and Lauritzen (2001) observed yet another type of nonlinearity, suggesting that a certain threshold of coordinated synaptic activity must be reached in order to trigger a hemodynamic response. Hence, synaptic activity needs to surpass a minimum threshold in order to cause an increase in CBF.

Overall, it appears that within a limited dynamic range of stimulus conditions, hemodynamic signals couple linearly to neuronal activity. In some parts of the brain or under certain stimulus conditions, however, this relationship takes on a nonlinear shape. Therefore, simply subtracting fMRI signal amplitudes obtained during two experimental conditions might not properly indicate the relative difference in underlying neuronal activity between these two states (Lauritzen 2005).

Interpreting fMRI data is complicated not only by the partially nonlinear relation between hemodynamics and neural activity but also by differences in the respective signal-to-noise ratio (SNR) of the two signals. The SNR of the neurophysiological signal associated with induced neuronal activity is about two orders of magnitude greater than that of the BOLD signal (Logothetis et al. 2001). Such a difference can, among other things, lead to statistical rejection ("false negatives") of valid activity during fMRI experiments, despite the fact that the underlying neural response is significant. These considerations are consistent with the finding that extensive averaging of fMRI data (which increases SNR) allows for more brain regions to be correctly classified as activated regions (Saad et al. 2003).

4.5 What Is the Neural Origin of fMRI Responses?

As indicated above, several studies have found a nearly linear relationship between metabolic and hemodynamic brain responses and local spiking activity. Specifically, Shmuel and Grinvald (1996) compared the optically measured reduction in blood oxygenation (the "initial dip") in the cat visual cortex to the concurrently elicited spiking response to visual stimuli of drifting gratings. They observed an approximately linear relationship between these two measures, indicating a correspondence between spiking responses and activity-dependent oxygen consumption during the initial, negative-going phase of the BOLD response, before the increase in CBF. Smith et al. (2002) recorded changes in cortical spiking activity during forepaw stimulation of anesthetized rats and found a similar connection between

oxygen consumption and spiking activity for the subsequent phase of the positive BOLD response when CBF is increased. They also measured the localized changes in oxygen consumption under the same conditions. The stimulus-induced changes in oxygen consumption were reported to be roughly proportional to the associated changes in spiking activity.

Rees et al. (2000) compared fMRI responses to visual motion stimuli in the motion-sensitive human area cortical MT+ to spiking responses obtained in monkey MT using matching stimuli. Responses in human MT+ showed a linear dependence on the coherence of motion signals, which mirrored similar changes in the rate of action potentials obtained in the animals using the same stimuli. Similar results were obtained by comparing BOLD responses in human V1 and action potential responses in monkey V1 to stimuli of varying brightness contrast (Heeger et al. 2000). These observations support the notion that fMRI responses of a cortical area are directly proportional to the average firing rate of its local cell population.

However, it is worth noting that synaptic activity is highly interrelated with the firing rates of pre-synaptic and post-synaptic neurons. This suggests that synaptic activity is also correlated with metabolic and hemodynamic responses. This assumption is particularly valid for the cerebral cortex, where the majority of synapses (both excitatory and inhibitory) originate locally, leaving only a minority of inputs from more remote cortical and subcortical structures (Braitenberg and Schuz 1991; Peters and Payne 1993; Peters and Sethares 1991). It thus seems reasonable to expect that an increase in local firing rates correlates with a comparative rise in local synaptic activity, which in turn leads to an increase in both the metabolic demand and vascular response.

Given the reasoning outlined above, it may not be surprising that in many cases, the BOLD signal has been found to correlate equally well with LFPs and spiking activity. For example, Mukamel et al. (2005) contrasted both single-unit activity and LFPs in the auditory cortex of two neurosurgical patients with the fMRI signals of healthy subjects during the presentation of an identical stimulus set. Their findings revealed a linear relationship between spiking activity, high-frequency LFPs, and the fMRI BOLD signal measured in the human auditory cortex. However, since the spiking activity was highly correlated with the high-frequency LFP, these results cannot answer the question regarding which of the two signals (LFP or spikes) has more predictive power for estimating the local BOLD response.

To summarize, the fMRI BOLD response can be taken as a dependable estimate of the average firing rate of the underlying neuronal population under a wide variety of stimulation conditions. Yet, correlation does not equal causation. The mere observation of close coupling between these signals does not imply that spiking activity drives (directly causes) the BOLD signal. One problem, in particular, is that the magnitude of local synaptic activity (and thus the resulting LFP) tends to be closely coupled with simultaneous changes in spike rate. In other words, it is difficult to attribute the relative roles of synaptic inputs versus the spiking output for hemodynamic changes given that both these processes tend to co-vary that closely. However, several studies managed to separate LFP and spiking responses in order to investigate their relative effects on the BOLD response.

Schwartz et al. (1979) measured localized brain-glucose metabolism in rats using 2-deoxyglucose autoradiography (Sokoloff et al. 1977). They subjected rats to an osmotic load that stimulated neuronal cell bodies in the supraoptic and paraventricular nuclei of the hypothalamus. The axon terminals of these neurons reside in the posterior pituitary gland, which is separated by a considerable distance from the stimulated cell bodies. The authors compared the metabolic activity in both locations and found that brain metabolism increased significantly in the area harboring the axon terminals (the posterior pituitary gland). In contrast, there were no measurable metabolism changes in the cell bodies residing in the hypothalamus. This finding is consistent with the known relationship between the metabolic cost of sustaining ionic gradients and the surface-area-to-volume ratio of neurons (Cohen and De Weer 1977; Ritchie 1967; Raichle and Mintum 2006). In general, their data support the notion that synaptic input, and not the spiking output, is the driving mechanism of localized changes in the brain metabolism (see Lauritzen (2005) for additional evidence).

Mathiesen et al. (1998) employed laser Doppler flow and extracellular neurophysiological recordings to differentiate between synaptic and spiking activities in order to investigate their relative impact on CBF in the rat cerebellum. Stimulation of the monosynaptic climbing fiber system triggered LFPs and complex spikes of Purkinje cells with concurrent increases in CBF. However, when spiking activity was inhibited, CBF increased despite the decrease in spiking activity (Fig. 4.5a). This discovery verified that activity-dependent CBF increases in the cerebellum depend on synaptic excitation and that the net spiking activity of Purkinje cells is insignificant for the vascular response.

Thomsen et al. (2004) examined the consequences of enhanced spiking activity on CBF in the rat cerebellum under conditions of disinhibition, which was achieved by blocking GABA (A) receptors with either bicuculline or picrotoxin. Disinhibition increased Purkinje cell spiking rates to 200–300% of control activity. However, there was no increase in basal CBF. This finding illustrates that increased spike activity alone is insufficient to affect CBF. In contrast, the neurovascular coupling between excitatory synaptic activity evoked by climbing fiber stimulation and CBF responses was maintained during disinhibition. Thus, increasing the spiking activity of principal neurons is neither sufficient nor necessary to elicit CBF responses. Instead, activation-dependent vascular signals seem to mainly reflect excitatory synaptic activity.

Logothetis et al. (2001) examined the relationship of the BOLD signal with LFPs and spiking activity in the monkey visual cortex. The largest increases in LFP power in response to visual stimulation were observed within the gamma frequency range (>30 Hz) of the LFPs. LFPs were found to reflect the time course of the BOLD response more accurately since both LFP power and BOLD tended to remain elevated for the duration of the visual stimulus, while spiking activity did not (Fig. 4.5b). Linear systems analysis revealed that LFPs yield a better approximation of the BOLD response than the spiking responses. A follow-up study in alert monkeys verified that LFPs are more accurate and more reliable predictors of the BOLD response, despite the fact that both LFPs and MUA correlate with the BOLD signal

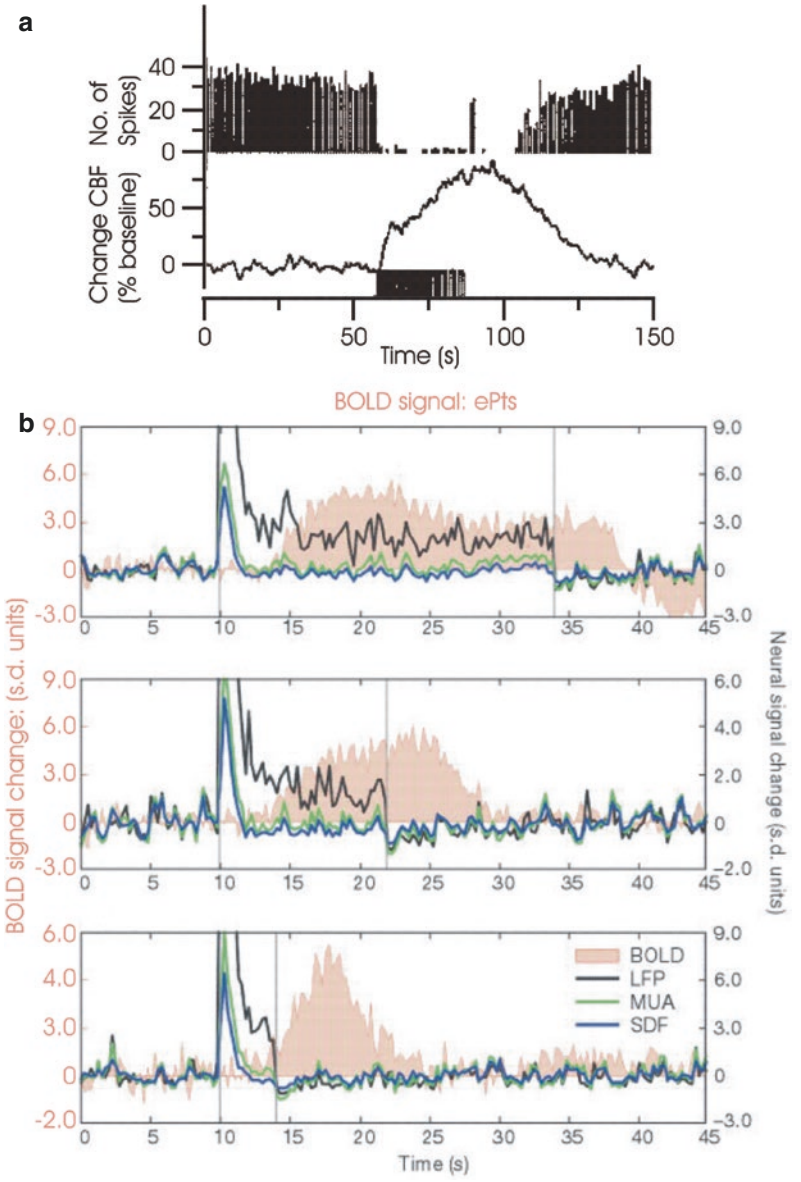

Fig. 4.5 CBF and BOLD responses correlate with LFPs. (**a**) Activity-dependent CBF increases and spike activity in response to parallel fiber stimulation in the cerebellum. Purkinje cell spiking activity diminished after 1–3 s of stimulation, and spontaneous firing did not return to baseline until 19–25 s after the end of stimulation (*upper plot*). CBF increased during stimulation and persisted for 5–10 s after the end of stimulation before returning to baseline after a lag of 40–50 s (*lower plot*). (Modified from Fig. 3a of Mathiesen et al. (1998) with permission). (**b**) Simultaneous neural and BOLD recordings from a cortical site showing a transient MUA response. Responses to a pulse stimulus of 4, 12, and 24 s are shown in the bottom, middle, and top plots, respectively. LFP is the sole signal showing time course matched in response to duration with that of the BOLD response. Both the spike density function (SDF) and the multi-unit activity (MUA) adapt back to baseline a couple of seconds after stimulus onset. The BOLD time series is from an ROI around the electrode. *CBF* cerebral blood flow, *ROI* region of interest. (Modified from Fig. 3 of Logothetis et al. (2001) with permission)

(Goense and Logothetis 2008). More recent work expanded this result by demonstrating that similar differences can be found in the rodent cortex, independently of whether local neural stimulation was achieved via sensory stimulation or optogenetic excitation (Iordanova et al. 2015). In either case, LFPs were well correlated with local cerebral blood flow, moderately with cerebral blood volume, and less correlated with blood oxygenation, while pre-synaptic firing rates had little impact on the vascular response.

Similar results were reported by Niessing et al. (2005), who recorded neurophysiological signals and optically measured hemodynamic responses in the cat visual cortex. Increasing visual stimulus strength resulted in enhanced spiking activity, high-frequency LFP power, and hemodynamic responses. However, hemodynamic responses were found to fluctuate when stimuli of constant intensity were presented to the animal. These fluctuations were only weakly related to the rate of action potentials. In contrast, they were tightly correlated with LFP power in the gamma range. When sorting the data according to the amplitude of the hemodynamic response, clear differences were detected with respect to the frequency distribution of the respective LFPs. Specifically, LFP power increases in the delta (~1–4 Hz), theta (~4–8 Hz), and alpha (~8–12 Hz) frequency bands were most prevalent for stimulus presentations that evoked the weakest hemodynamic responses. With the increasing hemodynamic response, the peak of LFP power shifted from the theta and alpha bands to the beta (~12–30 Hz) and lower gamma frequency bands. The strongest hemodynamic responses were linked to high power in the lower and upper gamma frequency bands. Quantifying the relationship between the strength of the hemodynamic response and LFP power in different frequency bands revealed that low-frequency activity in the delta band was negatively correlated with hemodynamic signal strength. Theta, alpha, and beta power levels were not significantly correlated with the vascular response. A weak and strong positive correspondence existed for LFP power in the lower and upper gamma bands, respectively. LFP power in the high-frequency range in particular is thought to increase with the local synaptic events, signifying a close association between hemodynamic responses and neuronal synchronization.

Viswanathan and Freeman (2007) demonstrated yet another dissociation between synaptic and spiking activities in the cat primary visual cortex. They presented visual stimuli composed of gratings that were drifting at different temporal frequencies. Simultaneously, they recorded neural responses and local tissue oxygenation that can serve as a proxy for the BOLD signal. Spiking activity decreased while LFP power in the lower gamma band became more prevalent when the temporal frequency of the gratings increased. Compared to their maximal responses, which were obtained at a stimulus frequency of 4 Hz, spiking activity and low-gamma LFPs dropped to approximately 15% and 85%, respectively, during visual stimulation at 20 Hz. LFP responses in the delta, theta, alpha, beta, and high-gamma bands plunged to approximately 40% of their maximal response at 4 Hz, while tissue oxygen fell to 60%. These results indicate the existence of close coupling between tissue oxygenation and LFP power, but not with spiking activity.

Interestingly, Bentley et al. (2016) found that oxygen responses were correlated with LFP power in different cortical areas of macaque monkeys, while the apparent hemodynamic coupling between the oxygen level and electrophysiology differed across areas. Specifically, they paired oxygen polarography, an electrode-based oxygen measurement technique, with standard electrophysiological recording to assess the relationship of oxygen and neural activity in two cortical areas: the task-negative posterior cingulate cortex (PCC) and the visually responsive task-positive area V3. Their finding suggests that cortical oxygen responses reflect concurrent changes in LFP power and that either the coupling of neural activity to blood flow and metabolism differs between areas or that computing a linear transformation from a single LFP band to the oxygen level does not capture the true physiological process.

Rauch et al. (2008) used an experimental dissociation between spiking and LFPs by injecting a neuromodulator that primarily acts on efferent neuronal membranes into the primary visual cortex of anesthetized monkeys. The neuromodulator reduced population spiking responses without significantly affecting either LFPs or BOLD activity, implying that the efferent neurons within the visual cortex pose a relatively small metabolic burden compared to the overall pre-synaptic and post-synaptic processing of incoming afferents. In other words, BOLD seems to predominantly reflect pre-synaptic and post-synaptic processing of incoming afferents to a particular cortical region.

So far, we have described both cases of coupling and of dissociation between spiking activity and the BOLD signal. Yet, the question remains: what determines whether the BOLD signal is associated with or dissociated from the spiking output of neurons in any specific paradigm? Using multiple electrodes in the human auditory cortex, Nir et al. (2007) measured spiking activity and LFPs and observed a wide range of coupling levels between the activity of individual neurons and gamma-range LFPs. The gamma LFPs were well correlated with BOLD signals measured across different individuals (r = 0.62). In contrast, the coupling of single-neuron spiking to BOLD responses was highly variable. However, the BOLD response was tightly related to interneuronal firing-rate correlations (r = 0.70). These results suggest that the BOLD signal could closely reflect spiking activity, depending on whether an experimental paradigm evokes a high degree of interneuronal correlation.

4.6 Neuronal Correlates of Negative BOLD Responses

Sustained negative responses are an interesting, pervasive phenomenon in functional brain imaging. Some hypotheses regarding the origin of these negative responses suggest a purely vascular basis for this phenomenon (such as "vascular blood steal"), concluding that the negative BOLD response (NBR) bears little relation to underlying neuronal activity (Harel et al. 2002; Kannurpatti and Biswal 2004). Shmuel et al. (2002) demonstrated a robust, sustained NBR in the human occipital cortex triggered by stimulating part of the visual field. This NBR was linked to decreases in CBF and consequently reductions in oxygen consumption. These results suggest that the NBR is associated with reductions in local neuronal activity. Similar links of NBRs to decreases in local CBF and oxygen consumption have been reported in the visual

(Uludağ et al. 2004; Pasley et al. 2007) and motor cortices (Stefanovic et al. 2004, 2005). In addition, Shmuel et al. (2006) employed a similar stimulation paradigm to the one they used in humans in the monkey primary visual cortex and obtained a similar NBR outside the stimulated brain regions. Using simultaneous fMRI and neurophysiological recordings, they then showed that the negative BOLD response was associated with local decreases in the neuronal activity below the baseline level of spontaneous activity. Trial-by-trial comparisons showed a tight coupling between the NBR and reduced neuronal activity. The NBR was linked to comparable decreases in LFPs and MUA. These findings indicate that a large component of the NBR stems from decreases in neuronal activity (Fig. 4.6).

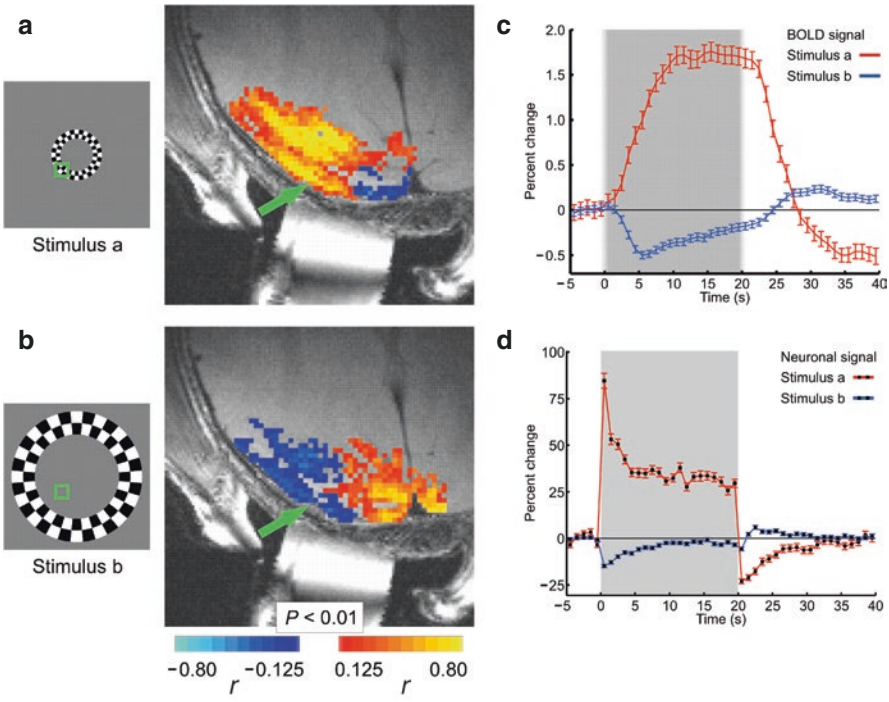

Fig. 4.6 Neuronal correlates of a negative BOLD response (NBR). (**a**, **b**) Patterns of response to a central and a peripheral visual field stimulus, respectively. The fMRI response from a single axial-oblique slice is superimposed on the corresponding anatomical image. *Green arrows* indicate the position of the recording electrode within visual area V1. *Green squares* represent the collective receptive field of the neurons in the vicinity of the electrode. The stimulus in (**a**) overlapped with the receptive field, invoking a positive BOLD response in the area directly surrounding the electrode. The stimulus in (**b**) did not overlap with the receptive field and induced an NBR in that same vicinity. (**c**) Time course (mean ± SEM) of the BOLD response sampled from the ROI around the electrode. (**d**) Neuronal responses to the stimuli presented in (**a**, **b**). Time courses (mean ± SEM) present the fractional change in power of the broad-band neuronal signal in response to stimuli that overlapped (*red*) or did not overlap (*blue*) with the receptive field. The data in (**c**, **d**) were averaged over all trials from 15 sessions. (All panels were modified from Shmuel et al. (2006) (Figs. 1a, b, and d and 2a) with permission)

The neuronal and vascular mechanisms underlying NBRs in rat primary somatosensory cortex were also studied by Devor et al. (2007) using optical imaging techniques. Stimulation of rat forepaws resulted in a central region of net depolarization surrounded by net hyperpolarization. Hemodynamic measurements revealed correspondence between the depolarized regions with an increase in local blood oxygenation, as well as an association between hyperpolarized cortical regions and decreased blood oxygenation. On the microscopic level of single arterioles, the vascular response was found to be composed of a combination of dilatory and constrictive phases. The relative amplitude of vasoconstriction co-varied with the strength of neuronal hyperpolarization and the corresponding decrease in oxygenation. These findings imply that neuronal inhibition and concomitant arteriolar vasoconstriction relate to decreased blood oxygenation, which would be consistent with a negative BOLD fMRI response.

Additional evidence linking negative BOLD responses to inhibited neuronal activity was demonstrated by Boorman et al. (2010). These authors employed electrical whisker-pad stimulation while imaging the rat somatosensory cortex. They demonstrated negative BOLD responses in deeper cortical layers. Separate two-dimensional optical imaging spectroscopy and laser Doppler flowmetry revealed that the NBR was the result of decreased blood volume and flow and increased levels of deoxyhemoglobin. Neural activity in the NBR region, measured with multichannel electrodes, varied considerably as a function of cortical depth. There was a decrease in neuronal activity in the deep cortical laminae. After cessation of whisker stimulation, there was a large increase in neural activity above baseline. Both the decrease in neuronal activity and the increase above baseline correlated well with the simultaneously measured blood flow, suggesting that the NBR is related to decreases in neural activity within the deep cortical layers.

4.7 Neuronal Correlates of Spontaneous Fluctuations in fMRI Signals

Early fMRI studies deemed the large cortical signal fluctuations that can be observed when a subject is resting without explicit stimulation or task instructions are just random, meaningless “noise.” However, more recent work has demonstrated that the spatio-temporal structure of these spontaneously occurring signal changes is not random at all. Instead, spontaneous fluctuations in BOLD are highly organized, and this spatial organization is consistent between subjects (Biswal et al. 1995; Fox and Raichle 2007). As a consequence, the relationship between BOLD and the underlying neural events in the resting state is of particular interest. These spontaneous fluctuations in fMRI signals are reminiscent of previously demonstrated spontaneous fluctuations in cortical neuronal signals observed in cats (Arieli et al. 1996) and monkeys (Leopold et al. 2003). Importantly, these resting-state fluctuations are correlated across large parts of the brain (Biswal et al. 1995), a phenomenon termed functional connectivity.

Several studies identified contributions of non-neuronal origins to spontaneous fluctuations in fMRI signals. These contributions include vascular vaso-motion (Mayhew et al. 1996) and respiration (Birn et al. 2006; Wise et al. 2004). However, there is also evidence for neural events giving rise to resting-state functional connectivity. Shmuel and Leopold (2008) obtained simultaneous fMRI and intracortical neurophysiological recordings in anesthetized, paralyzed monkeys that were either exposed to a uniform grey field or to complete darkness. They found an association between slow fluctuations in the spontaneous BOLD signals and concurrent fluctuations in the underlying local neuronal activity. This correlation varied with the BOLD signal time-lag relative to neuronal activity, resembling a traditional hemodynamic response function with peaks at a 6-s lag of the BOLD signal (Fig. 4.7a–j). These associations were consistently identified when the neuronal signal consisted of either relative power variations in the LFPs gamma band, MUA, or the spiking rate of a small group of neurons. Further examination of the relationship between the fMRI time series of different parts of the cortex and the neuronal activity measured within one cortical site revealed that widespread areas of the visual cortex in both hemispheres were significantly correlated with neuronal activity from a single recording site in area V1 (Fig. 4.7k). Assuming that Shmuel and Leopold's (2008) results from area V1 can be generalized to other cortical areas, fMRI-based functional connectivity between remote regions in the resting state can be linked to the synchronization of slow fluctuations in the underlying neuronal signals.

Schölvinck et al. (2010) replicated and expanded on these results using alert monkeys. Their results demonstrate widespread, positive correlations of fMRI signals over nearly the entire cerebral cortex with the spontaneous fluctuations in the LFPs measured at a single cortical site (Fig. 4.7). The spontaneous neural activity reported in that study accounted for 10% of the observed BOLD signal variance, which is a considerable fraction of the 50% explained variance during visual stimulation. Similar to the findings by Shmuel and Leopold (2008), the observed correlation was especially consistent for upper gamma-range frequencies (40–80 Hz; Fig. 4.7m). A strong, positive correlation was also detected in a band of lower frequencies (2–15 Hz), albeit with a lag closer to zero. Overall, these findings specify that the global constituent of fMRI fluctuations measured during the resting state is closely linked to neural activity.

Hutchison et al. (2015) uncovered similar results for the monkey prefrontal cortex. They measured both fMRI BOLD responses and LFPs in anesthetized animals that were not exposed to any explicit sensory stimulation. They also found that high-frequency LFPs were correlated with BOLD activity at the recording site, while low-frequency LFPs were not. They further showed that high-frequency (i.e., beta to low gamma) and low-frequency (i.e., delta to theta) LFP power were anti-correlated in the absence of any explicit stimuli. This finding corroborates the notion that complementary changes in low- and high-frequency bands are an intrinsic property of LFPs and explains why low- and high-frequency LFPs yield different correlations with the fMRI BOLD response.

Using an electrophysiology system that can record the full band of LFPs, Pan et al. (2013) demonstrated that in addition to correlation with the power of

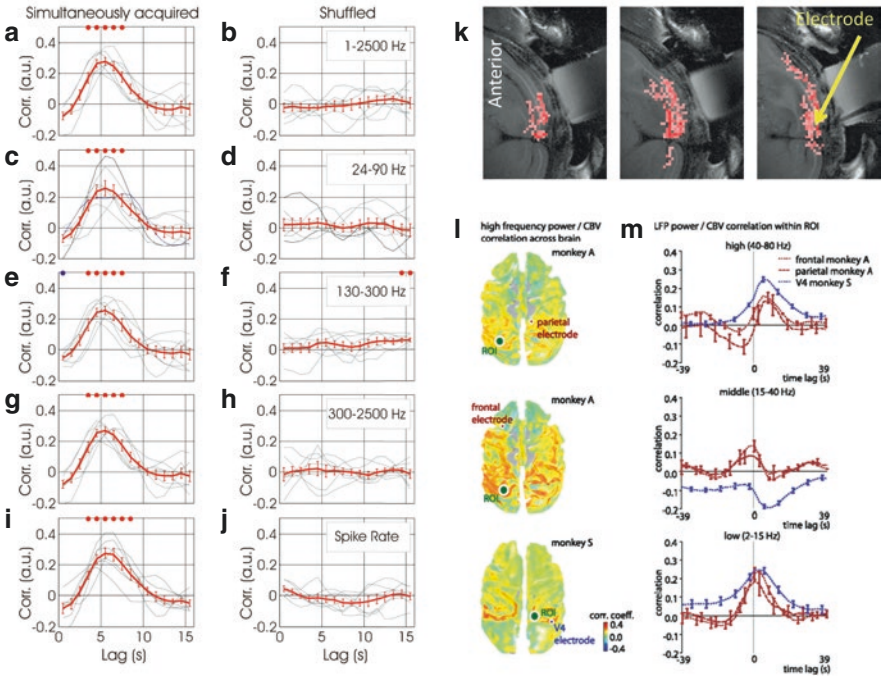

Fig. 4.7 Spontaneous fluctuations in BOLD signal correlate with the underlying neurophysiological activity. (**a**–**i**) Co-variation between spontaneous fluctuations in fMRI and neuronal signals as a function of temporal lag. (**a**) The grey curves show the correlation as a function of lag from each experiment. The red curve presents the correlation function averaged over seven experiments in five different monkeys (mean ± SEM). The vertical axis represents Spearman's correlation coefficient between BOLD and the fluctuations in relative (fractional change) power averaged over frequencies of the denoised broad-band neurophysiological signal acquired simultaneously with fMRI. The horizontal axis represents the lag between the two correlated signals, with positive lags standing for BOLD lagging behind the neuronal activity. (**b**) Correlation between the same signals as presented in (**a**), computed after breaking the simultaneity condition by shuffling the segments of BOLD and neuronal activity obtained within each experiment. (**c**–**h**) present correlation functions in the format used for (**a**) and (**b**), for the LFP, mid-range, and MUA bands, respectively. (**i**, **j**) present similar correlation functions for fluctuations in spiking activity, estimated by counting identified action potentials over 1 s epochs rather than using frequency-based analysis. (Modified from Shmuel and Leopold (2008), with permission). (**k**) Spatial extent of the correlation between the slow relative fluctuations in power averaged over frequencies of the broad-band neuronal signal recorded at the tip of the electrode (yellow arrow) and the fluctuations in BOLD measured voxel by voxel. Pink-colored voxels showed a statistically significant positive correlation between the neurophysiological activity recorded in one site in V1 and BOLD signals for a 5 s time-lag (*t*-test, averaging over the correlation obtained time-segment by time-segment, $p < 0.01$). (Modified from Shmuel and Leopold (2008), with permission). (**l**, **m**) Spatial extent of the fMRI correlation with high-frequency LFP in frontal area 6d, parietal area 7a, and occipital area V4. (**l**) In all cases, spatial correlations are bilateral and spread over large swathes of the cerebral cortex. (**m**) Cross-correlation functions between the fMRI and LFP power time courses for three electrodes outside V1 and for the three LFP frequency ranges: low (2–15 Hz), middle (15–40 Hz), and high (40–80 Hz). (Modified from Schölvinck et al. (2010), with permission). *CBV* cerebral blood volume, *LFP* local field potential

high-frequency LFPs, spontaneous fluctuations in BOLD signals also correlate with infra-slow, 0.05–0.25 Hz components of the neural signals.

4.8 Dissociations Between BOLD Responses and Neurophysiological Activity

The previous sections focused on cases where metabolic and hemodynamic responses largely corresponded to changes in neurophysiological activity. A few studies reported cases where these signals dissociated. Maier et al. (2008) investigated brain responses to a visual illusion in which a part of an image can become subjectively invisible. Perceptual disappearance of the visual stimulus elicited a robust drop in V1 fMRI signal in humans. In contrast, monkey single-neuron recordings failed to demonstrate such perception-related changes in V1 spiking. To investigate the basis of this discrepancy, they next measured both the BOLD response and electrophysiological signals. They found that all signals were in good agreement during conventional stimulus presentation, showing strong modulation to the presentation and removal of a visual stimulus. During perceptual suppression, however, only the BOLD response and low-frequency (5–30 Hz) LFP power showed decreases, whereas both spiking and high-frequency LFP power remained unaffected. These results demonstrate that the coupling between BOLD and electrophysiological signals in V1 is context-dependent, with a marked dissociation occurring during a state of perceptual suppression.

While Maier et al. (2008) observed changes in lower LFP frequency bands that corresponded to the BOLD signal, Sirotin and Das (2009) found evidence of a complete divergence of hemodynamic and neurophysiological signals. Using a dual-wavelength optical imaging technique that independently measured cerebral blood volume and oxygenation, they found two distinct components of the hemodynamic signal in V1 of alert animals. One component was reliably predictable from neuronal responses to visual stimulation. The other component, of almost comparable strength, was reported as an unknown signal that entrained to task structure of rhythmic stimulus presentations independently of visual input or of standard neural predictors of hemodynamics. The resulting data exhibited robust modulations of the hemodynamic signal at the stimulus presentation frequency, even though the animals were in complete darkness. This latter component showed predictive timing, with increases in cerebral blood volume in anticipation of future stimulus onsets. Sirotin and Das (2009) suggested the existence of a preparatory mechanism that brings additional arterial blood to the cortex in anticipation of expected tasks. This mechanism could be implemented via distal neuromodulatory control of cerebral arteries. This interpretation was challenged by several authors (e.g., Logothetis (2010) and Handwerker and Bandettini (2011)), indicating that the data presented by Sirotin and Das (2009) did show modulation of neuronal activity in V1, likely reducing spontaneous activity during fixation. The increased inhibition, visible in their spectrograms, may trigger CBV changes and yield anticipatory responses. It was hypothesized that the responses are due to site-specific effects of neuromodulatory input on the cortical

excitation-inhibition balance, mediated by norepinephrine released from the locus coeruleus. Others (e.g., Tan 2009) supported the findings and interpretation of Sirotin and Das (2009) and suggested that the task-related properties of these responses point to a possible link between regional cerebral microcirculation and dopaminergic signaling. It was hypothesized that dopamine plays a role in the task-dependent, "on-demand" allocation of metabolic resources.

It should be noted that both Maier et al. (2008) and Sirotin and Das (2009) pursued their measurements in alert animals, while the majority of other studies of neurovascular coupling used anesthetized animals. Neurovascular coupling depends on the state of the animal—alert or anesthetized (Paasonen et al. 2018)—and on the anesthesia regime (Franceschini et al. 2010; Paasonen et al. 2018; Bortel et al. 2020). The findings by Maier et al. (2008) and Sirotin and Das (2009) indicate that neurovascular coupling may be modified in the alert state, possibly via the action of neuromodulators that depend on behavioral state. This adds to the complexity of the interplay between neurophysiological signals and hemodynamic responses, which remains to be addressed in future studies.

References

Arieli A, Sterkin A, Grinvald A, Aertsen A (1996) Dynamics of ongoing activity: explanation of the large variability in evoked cortical responses. Science 273:1868–1871

Arthurs OJ, Boniface SJ (2003) What aspect of the fMRI BOLD signal best reflects the underlying electrophysiology in human somatosensory cortex? Clin Neurophysiol 114:1203–1209

Bandettini PA, Wong EC, Hinks RS, Tikofsky RS, Hyde JS (1992) Time course EPI of human brain function during task activation. Magn Reson Med 25:390–397

Bannister AP (2005) Inter- and intra-laminar connections of pyramidal cells in the neocortex. Neurosci Res 53:95–103

Bastos AM, Loonis R, Kornblith S, Lundqvist M, Miller EK (2018) Laminar recordings in frontal cortex suggest distinct layers for maintenance and control of working memory. Proc Natl Acad Sci U S A 115(5):1117–1122

Bentley WJ, Li JM, Snyder AZ, Raichle ME, Snyder LH (2016) Oxygen level and LFP in task-positive and task-negative areas: bridging BOLD fMRI and electrophysiology. Cereb Cortex 26(1):346–357

Billings-Gagliardi S, Chan-Palay V, Palay SL (1974) A review of lamination in area 17 of the visual cortex Macaca mulatta. J Neurocytol 3:619–629

Birn RM, Diamond JB, Smith MA, Bandettini PA (2006) Separating respiratory-variation-related fluctuations from neuronal-activity-related fluctuations in fMRI. Neuroimage 31:1536–1548

Biswal B, Yetkin FZ, Haughton VM, Hyde JS (1995) Functional connectivity in the motor cortex of resting human brain using echo-planar MRI. Magn Reson Med 34:537–541

Bode-Greuel KM, Singer W, Aldenhoff JB (1987) A current source density analysis of field potentials evoked in slices of visual cortex. Exp Brain Res 69:213–219

Bollimunta A, Chen Y, Schroeder CE, Ding M (2008) Neuronal mechanisms of cortical alpha oscillations in awake-behaving macaques. J Neurosci. 28:9976–9988

Boorman L, Kennerley AJ, Johnston D, Jones M, Zheng Y, Redgrave P, Berwick J (2010) Negative blood oxygen level dependence in the rat: a model for investigating the role of suppression in neurovascular coupling. J Neurosci 30:4285–4294

Bortel A, Pilgram R, Yao Z-S, Shmuel A (2020) Dexmedetomitine—commonly used in functional imaging studies—increases susceptibility to seizures in rats but not in wild type mice. Front Neurosci 14:832. https://doi.org/10.3389/fnins.2020.00832

Braitenberg V, Schuz A (1991) Anatomy of the cortex. Springer, Berlin
Brinker G, Bock C, Busch E, Krep H, Hossmann KA, Hoehn-Berlage M (1999) Simultaneous recording of evoked potentials and T2*-weighted MR images during somatosensory stimulation of rat. Magn Reson Med 41:469–473
Buffalo EA, Fries P, Landman R, Buschman TJ, Desimone R (2011) Laminar differences in gamma and alpha coherence in the ventral stream. Proc Natl Acad Sci U S A 108:11262–11267
Buxton RB, Uludag K, Dubowitz DJ, Liu TT (2004) Modeling the hemodynamic response to brain activation. Neuroimage 23:S220–S233
Chaimow D, Yacoub E, Uğurbil K, Shmuel A (2018) Spatial specificity of the functional MRI blood oxygenation response relative to neuronal activity. Neuroimage 164:32–47
Cohen LB, De Weer P (1977) Structural and metabolic processes directly related to action potential propagation. In: Brookhart JM, Mountcastle VB (eds) Handbook of physiology: the nervous system. American Physiological Society, Bethesda, pp 137–159
Cox MA, Dougherty K, Adams GK, Reavis EA, Westerberg JA, Moore BS, Leopold DA, Maier A (2019) Spiking suppression precedes cued attentional enhancement of neural responses in primary visual cortex. Cereb Cortex 29(1):77–90
DeFelipe J, Alonso-Nanclares L, Arellano JI (2002) Microstructure of the neocortex: comparative aspects. J Neurocytol 31:299–316
Devor A, Dunn AK, Andermann ML, Ulbert I, Boas DA, Dale AM (2003) Coupling of total hemoglobin concentration, oxygenation, and neural activity in rat somatosensory cortex. Neuron 39:353–359
Devor A, Tian P, Nishimura N, Teng IC, Hillman EMC, Narayanan SN, Ulbert I, Boas DA, Kleinfeld D, Dale AM (2007) Suppressed neuronal activity and concurrent arteriolar vasoconstriction may explain negative blood oxygenation level-dependent signal. J Neurosci 27:4452–4459
Dougherty K, Cox MA, Ninomiya T, Leopold DA, Maier A (2017) Ongoing alpha activity in V1 regulates visually driven spiking responses. Cereb Cortex 27(2):1113–1124
Douglas RJ, Martin KAC (2004) Neuronal circuits of the neocortex. Annu Rev Neurosci 27:419–451
Douglas RJ, Martin KAC, Whitteridge D (1989) A canonical microcircuit for neocortex. Neural Comput 1:480–488
Engel SA, Glover GH, Wandell BA (1997) Retinotopic organization in human visual cortex and the spatial precision of functional MRI. Cereb Cortex 7:181–192
Engel TA, Steinmetz NA, Gieselmann MA, Thiele A, Moore T, Boahen K (2016) Selective modulation of cortical state during spatial attention. Science 354(6316):1140–1144
Felleman DJ, Van Essen DC (1991) Distributed hierarchical processing in the primate cerebral cortex. Cereb Cortex 1:1–47
Fox PT, Raichle ME (1986) Focal physiological uncoupling of cerebral blood-flow and oxidative-metabolism during somatosensory stimulation in human-subjects. Proc Natl Acad Sci U S A 83:1140–1144
Fox MD, Raichle ME (2007) Spontaneous fluctuations in brain activity observed with functional magnetic resonance imaging. Nat Rev Neurosci 8(9):700–711
Franceschini MA, Radhakrishnan H, Thakur K, Wu W, Ruvinskaya S, Carp S, Boas DA (2010) The effect of different anesthetics on neurovascular coupling. Neuroimage 51:1367–1377
Freeman WJ (1975) Mass action in the nervous system. Academic, New York
Goense JBM, Logothetis NK (2008) Neurophysiology of the BOLD fMRI signal in awake monkeys. Curr Biol 18:631–640
Goense J, Bohraus Y, Logothetis NK (2016) fMRI at high spatial resolution: implications for BOLD-models. Front Comput Neurosci 10:66
Handwerker DA, Bandettini PA (2011) Hemodynamic signals not predicted? Not so: a comment on Sirotin and Das (2009). Neuroimage 55(4):1409–1412
Hansen BJ, Dragoi V (2011) Adaptation-induced synchronization in laminar cortical circuits. Proc Natl Acad Sci U S A 108:10720–10725

Harel N, Lee SP, Nagaoka T, Kim DS, Kim SG (2002) Origin of negative blood oxygenation level-dependent fMRI signals. J Cereb Blood Flow Metab 22:908–917

Haug H (1987) Brain sizes, surfaces, and neuronal sizes of the cortex cerebri: a stereological investigation of man and his variability and a comparison with some mammals (primates, whales, marsupials, insectivores, and one elephant). Am J Anat 180:126–142

Heeger DJ, Huk AC, Geisler WS, Albrecht DG (2000) Spikes versus BOLD: what does neuroimaging tell us about neuronal activity? Nat Neurosci 3:631–633

Hembrook-Short JR, Mock VL, Briggs F (2017) Attentional modulation of neuronal activity depends on neuronal feature selectivity. Curr Biol 27(13):1878–1887.e5

Herculano-Houzel S, Collins CE, Wong P, Kaas JH, Lent R (2008) The basic nonuniformity of the cerebral cortex. Proc Natl Acad Sci U S A 105:12593–12598

Hoffmeyer HW, Enager P, Thomsen KJ, Lauritzen MJ (2007) Nonlinear neurovascular coupling in rat sensory cortex by activation of transcallosal fibers. J Cereb Blood Flow Metab 27:575–585

Hoge RD, Atkinson J, Gill B, Crelier GR, Marrett S, Pike GB (1999) Linear coupling between cerebral blood flow and oxygen consumption in activated human cortex. Proc Natl Acad Sci U S A 96:9403–9408

Horton JC, Adams DL (2005) The cortical column: a structure without a function. Philos Trans R Soc Lond B Biol Sci 360:837–862

Hubel DH, Wiesel TN (1974) Uniformity of monkey striate cortex: a parallel relationship between field size, scatter, and magnification factor. J Comp Neurol 158:295–305

Huber L, Handwerker DA, Jangraw DC, Chen G, Hall A, Stüber C, Gonzalez-Castillo J, Ivanov D, Marrett S, Guidi M, Goense J, Poser BA, Bandettini PA (2017) High-resolution CBV-fMRI allows mapping of laminar activity and connectivity of cortical input and output in human M1. Neuron 96:1253–1263

Hutchison RM, Hashemi N, Gati JS, Menon RS, Everling S (2015) Electrophysiological signatures of spontaneous BOLD fluctuations in macaque prefrontal cortex. Neuroimage. 113:257–267

Iordanova B, Vazquez AL, Poplawsky AJ, Fukuda M, Kim SG (2015) Neural and hemodynamic responses to optogenetic and sensory stimulation in the rat somatosensory cortex. J Cereb Blood Flow Metab 6:922–932

Jones M, Hewson-Stoate N, Martindale J, Redgrave P, Mayhew J (2004) Nonlinear coupling of neural activity and CBF in rodent barrel cortex. Neuroimage 22:956–965

Juergens E, Guettler A, Eckhorn R (1999) Visual stimulation elicits locked and induced gamma oscillations in monkey intracortical- and EEG-potentials, but not in human EEG. Exp Brain Res 129:247–259

Kannurpatti SS, Biswal BB (2004) Negative functional response to sensory stimulation and its origins. J Cereb Blood Flow Metab 24:703–712

Klein C, Evrard HC, Shapcott KA, Haverkamp S, Logothetis NK, Schmid MC (2016) Cell-targeted optogenetics and electrical microstimulation reveal the primate koniocellular projection to supra-granular visual cortex. Neuron 90(1):143–151

Kwong KK, Belliveau JW, Chesler DA, Goldberg IE, Weisskoff RM, Poncelet BP, Kennedy DN, Hoppel BE, Cohen MS, Turner R, Cheng HM, Brady TJ, Rosen BR (1992) Dynamic magnetic resonance imaging of human brain activity during primary sensory stimulation. Proc Natl Acad Sci U S A 89:5675–5679

Lauritzen M (2005) Reading vascular changes in brain imaging: is dendritic calcium the key? Nat Rev Neurosci 6:77–85

Lawrence SJD, Formisano E, Muckli L, de Lange FP (2017) Laminar fMRI: applications for cognitive neuroscience. Neuroimage 197:785–791. S1053-8119(17)30572-4

Leopold DA, Murayama Y, Logothetis NK (2003) Very slow activity fluctuations in monkey visual cortex: implications for functional brain imaging. Cereb Cortex 13:423–433

Logothetis NK (2002) The neural basis of the blood-oxygen-level-dependent functional magnetic resonance imaging signal. Philos Trans R Soc Lond B 357:1003–1037

Logothetis NK (2010) Neurovascular uncoupling: much ado about nothing. Front Neuroenergetics 2:2

Logothetis NK, Pauls J, Augath M, Trinath T, Oeltermann A (2001) Neurophysiological investigation of the basis of the fMRI signal. Nature 412:150–157
Lübke J, Feldmeyer D (2007) Excitatory signal flow and connectivity in a cortical column: focus on barrel cortex. Brain Struct Funct 212:3–17
Maier A, Wilke M, Aura C, Zhu C, Ye FQ, Leopold DA (2008) Divergence of fMRI and neural signals in V1 during perceptual suppression in the awake monkey. Nat Neurosci 11(10):1193–1200
Maier A, Adams GK, Aura C, Leopold DA (2010) Distinct superficial and deep laminar domains of activity in the visual cortex during rest and stimulation. Front Syst Neurosci 4:31. https://doi.org/10.3389/fnsys.2010.00031
Maier A, Aura CJ, Leopold DA (2011) Infragranular sources of sustained local field potential responses in macaque primary visual cortex. J Neurosci 31:1971–1980
Maier A, Cox MA, Dougherty K, Moore B, Leopold D (2014) Anisotropy of ongoing neural activity in the primate visual cortex. Eye Brain 6(Suppl 1):113–120
Marín-Padilla M (1998) Cajal-Retzius cells and the development of the neocortex. Trends Neurosci 21:64–71
Mathiesen C, Caesar K, Akgoren N, Lauritzen M (1998) Modification of activity dependent increases of cerebral blood flow by excitatory synaptic activity and spikes in rat cerebellar cortex. J Physiol (Lond) 512:555–566
Maunsell JH, Gibson JR (1992) Visual response latencies in striate cortex of the macaque monkey. J Neurophysiol 68:1332–1344
Mayhew JE, Askew S, Zheng Y, Porrill J, Westby GW, Redgrave P, Rector DM, Harper RM (1996) Cerebral vasomotion: a 0.1-Hz oscillation in reflected light imaging of neural activity. Neuroimage 4:183–193
Mittmann W, Wallace DJ, Czubayko U, Herb JT, Schaefer AT, Looger LL, Denk W, Kerr JND (2011) Two-photon calcium imaging of evoked activity from L5 somatosensory neurons in vivo. Nat Neurosci 14:1089–1093
Mitzdorf U (1987) Properties of the evoked potential generators: current source-density analysis of visually evoked potentials in the cat cortex. Int J Neurosci 33:33–59
Mukamel R, Gelbard H, Arieli A, Hasson U, Fried I, Malach R (2005) Coupling between neuronal firing, field potentials, and fMR1 in human auditory cortex. Science 309:951–954
Nandy AS, Nassi JJ, Reynolds JH (2017) Laminar organization of attentional modulation in macaque visual area V4. Neuron 93(1):235–246
Nelson S (2002) Cortical microcircuits: diverse or canonical? Neuron 36:19–27
Nicholson C (1973) Theoretical analysis of field potentials in anisotropic ensembles of neuronal elements. IEEE Trans Biomed Eng 20:278–288
Nielsen A, Lauritzen M (2001) Coupling and uncoupling of activity-dependent increases of neuronal activity and blood flow in rat somatosensory cortex. J Physiol (Lond) 533:773–785
Niessing J, Ebisch B, Schmidt KE, Niessing M, Singer W, Galuske RA (2005) Hemodynamic signals correlate tightly with synchronized gamma oscillations. Science 309:948–951
Ninomiya T, Dougherty K, Godlove DC, Schall JD, Maier A (2015) Microcircuitry of agranular frontal cortex: contrasting laminar connectivity between occipital and frontal areas. J Neurophysiol 113(9):3242–3255
Nir Y, Fisch L, Mukamel R, Gelbard-Sagiv H, Arieli A, Fried I, Malach R (2007) Coupling between neuronal firing rate, gamma LFP, and BOLD fMRI is related to interneuronal correlations. Curr Biol 17:1275–1285
Nowak LG, Munk MH, Girard P, Bullier J (1995) Visual latencies in areas V1 and V2 of the macaque monkey. Vis Neurosci 12:371–384
Ogawa S, Lee TM, Kay AR, Tank DW (1990) Brain magnetic resonance imaging with contrast dependent on blood oxygenation. Proc Natl Acad Sci U S A 87:9868–9872
Ogawa S, Tank DW, Menon R, Ellermann JM, Kim SG, Merkle H, Ugurbil K (1992) Intrinsic signal changes accompanying sensory stimulation: functional brain mapping with magnetic-resonance-imaging. Proc Natl Acad Sci U S A 89:5951–5955
Paasonen J, Stenroos P, Salo RA, Kiviniemi V, Grohn O (2018) Functional connectivity under six anesthesia protocols and the awake condition in rat brain. Neuroimage 172:9–20

Pan W-J, Thompson GJ, Magnuson ME, Jaeger D, Keilholz S (2013) Infraslow LFP correlates to resting-state fMRI BOLD signals. Neuroimage 74:288–297
Pasley BN, Inglis BA, Freeman RD (2007) Analysis of oxygen metabolism implies a neural origin for the negative BOLD response in human visual cortex. Neuroimage 36:269–276
Pedemonte M, Barrenechea C, Nunez A, Gambini JP, Garcia-Austt E (1998) Membrane and circuit properties of lateral septum neurons: relationships with hippocampal rhythms. Brain Res 800:145–153
Peters A, Payne BR (1993) Numerical relationships between geniculocortical afferents and pyramidal cell modules in cat primary visual cortex. Cereb Cortex 3:69–78
Peters A, Sethares CJ (1991) Organization of pyramidal neurons in area 17 of monkey visual cortex. J Comp Neurol 306:1–23
Polimeni JR, Fischl B, Greve DN, Wald LL (2010) Laminar analysis of 7T BOLD using an imposed spatial activation pattern in human V1. Neuroimage 52:1334–1346
Raichle ME, Mintum MA (2006) Brain work and brain imaging. Annu Rev Neurosci 29:449–476
Rakic P (2008) Confusing cortical columns. Proc Natl Acad Sci U S A 105:12099–12100
Rauch A, Rainer G, Logothetis NK (2008) The effect of a serotonin-induced dissociation between spiking and perisynaptic activity on BOLD functional MRI. Proc Natl Acad Sci U S A 105:6759–6764
Rees G, Friston K, Koch C (2000) A direct quantitative relationship between the functional properties of human and macaque V5. Nat Neurosci 3:716–723
Ritchie JM (1967) The oxygen consumption of mammalian non-myelinated nerve fibers at rest and during activity. J Physiol (Lond) 188:309–329
Rockel AJ, Hiorns RW, Powell TP (1980) The basic uniformity in structure of the neocortex. Brain 103:221–244
Rockland KS, Drash GW (1996) Collateralized divergent feedback connections that target multiple cortical areas. J Comp Neurol 373:529–548
Saad ZS, Ropella KM, DeYoe EA, Bandettini PA (2003) The spatial extent of the BOLD response. Neuroimage 19:132–144
Sajad A, Godlove DC, Schall JD (2019) Cortical microcircuitry of performance monitoring. Nat Neurosci 2:265–274
Schölvinck M, Maier A, Ye F, Duyn J, Leopold DA (2010) Neural basis of global resting-state fMRI activity. Proc Natl Acad Sci U S A 107(22):10238–10243
Schroeder CE, Mehta AD, Givre SJ (1998) A spatiotemporal profile of visual system activation revealed by current source density analysis in the awake macaque. Cereb Cortex 8:575–592
Schwartz WJ, Smith CB, Davidsen L, Savaki H, Sokoloff L et al. (1979) Metabolic mapping of functional activity in the hypothalamo-neurohypophysial system of the rat. Science 205:723–725
Self MW, van Kerkoerle T, Goebel R, Roelfsema PR (2019) Benchmarking laminar fMRI: neuronal spiking and synaptic activity during top-down and bottom-up processing in the different layers of cortex. Neuroimage 197:806–817. S1053-8119(17)30517-7
Sheth SA, Nemoto M, Guiou M, Walker M, Pouratian N, Toga AW (2004) Linear and nonlinear relationships between neuronal activity, oxygen metabolism, and hemodynamic responses. Neuron 42:347–355
Shmuel A, Grinvald A (1996) Functional organization for direction of motion and its relationship to orientation maps in cat area 18. J Neurosci 16:6945–6964. and cover illustration
Shmuel A, Leopold DA (2008) Neuronal correlates of spontaneous fluctuations in fMRI signals in monkey visual cortex: implications for functional connectivity at rest. Hum Brain Mapp 29:751–761
Shmuel A, Yacoub E, Pfeuffer J, Van de Moortele PF, Adriany G, Hu XP, Ugurbil K (2002) Sustained negative BOLD, blood flow and oxygen consumption response and its coupling to the positive response in the human brain. Neuron 36:1195–1210
Shmuel A, Augath M, Oeltermann A, Logothetis NK (2006) Negative functional MRI response correlates with decreases in neuronal activity in monkey visual area V1. Nat Neurosci 9:569–577

Shmuel A, Yacoub E, Chaimow D, Logothetis NK, Ugurbil K (2007) Spatio-temporal point-spread function of fMRI signal in human gray matter at 7 Tesla. Neuroimage 35:539–552

Silberberg G, Gupta A, Markram H (2002) Stereotypy in neocortical microcircuits. Trends Neurosci 25:227–230

Sirotin YB, Das A (2009) Anticipatory haemodynamic signals in sensory cortex not predicted by local neuronal activity. Nature 457(7228):475–479

Smith AJ, Blumenfeld H, Behar KL, Rothman DL, Shulman RG, Hyder F (2002) Cerebral energetics and spiking frequency: the neurophysiological basis of fMRI. Proc Natl Acad Sci U S A 99:10765–10770

Snodderly DM, Gur M (1995) Organization of striate cortex of alert, trained monkeys (Macaca fascicularis): ongoing activity, stimulus selectivity, and widths of receptive field activating regions. J Neurophys 74:2100–2125

Sokoloff L, Reivich M, Kennedy C, Des Rosiers MH, Patlak CS, Pettigrew KD, Sakurada O, Shinohara M (1977) The [14C] deoxyglucose method for the measurement of local glucose utilization: theory, procedure and normal values in the conscious and anesthetized albino rat. J Neurochem 28:897–916

Sotero RC, Bortel A, Martínez-Cancino R, Neupane S, O'Connor P, Carbonell F, Shmuel A (2010) Anatomically-constrained effective connectivity among layers in a cortical column modeled and estimated from local field potentials. J Integr Neurosci 9:355–379

Sotero RC, Bortel A, Naaman S, Mocanu VM, Kropf P, Villeneuve MY, Shmuel A (2015) Laminar distribution of phase-amplitude coupling of spontaneous current sources and sinks. Front Neurosci 9:454

Stefanovic B, Warnking JM, Pike GB (2004) Hemodynamic and metabolic responses to neuronal inhibition. Neuroimage 22:771–778

Stefanovic B, Warnking JM, Kobayashi E, Bagshaw AP, Hawco C, Dubeau F, Gotman J, Pike GB (2005) Hemodynamic and metabolic responses to activation, deactivation and epileptic discharges. Neuroimage 28:205–215

Stephan KE, Petzschner FH, Kasper L, Bayer J, Wellstein KV, Stefanics G, Pruessmann KP, Heinzle J (2019) Laminar fMRI and computational theories of brain function. Neuroimage 197:699–706. S1053-8119(17)30908-4

Tan CA (2009) Anticipatory changes in regional cerebral hemodynamics: a new role for dopamine? J Neurophysiol 101:2738–2740

Thomsen K, Offenhauser N, Lauritzen M (2004) Principle neuron spiking: neither necessary nor sufficient for cerebral blood flow at rest or during activation in rat cerebellum. J Physiol (Lond) 560:181–189

Thomson AM, Bannister AP (2003) Interlaminar connections in the neocortex. Cereb Cortex 13:5–14

Trampel R, Bazin PL, Pine K, Weiskopf N (2019) In-vivo magnetic resonance imaging (MRI) of laminae in the human cortex. Neuroimage 197:707–715. S1053-8119(17)30785-1

Uludağ K, Dubowitz DJ, Yoder EJ, Restom K, Liu TT, Buxton RB (2004) Coupling of cerebral blood flow and oxygen consumption during physiological activation and deactivation measured with fMRI. Neuroimage 23:148–155

van Kerkoerle T, Self MW, Roelfsema PR (2017) Layer-specificity in the effects of attention and working memory on activity in primary visual cortex. Nat Commun. 8:13804

Viswanathan A, Freeman RD (2007) Neurometabolic coupling in cerebral cortex reflects synaptic more than spiking activity. Nat Neurosci 10:1308–1312

Wise RJS, Ide K, Poulin MJ, Tracey I (2004) Resting state fluctuations in arterial carbon dioxide induce significant low frequency variations in BOLD signal. Neuroimage 21:1652–1664